

**Electronic Supplementary Information**  
**Strain Buffering Effect of Quasi-Amorphous Disordered Microstructure**  
**Enabling Long-Term Fast Sodium Storage Performance**

Qiming He<sup>a,b</sup>, Sanpei Zhang<sup>a</sup>, Xiangwei Wu<sup>a,b</sup>, Jianhua Yang<sup>a,b</sup> and Zhaoyin Wen<sup>\*a,b</sup>

<sup>a</sup> CAS Key Laboratory of Materials for Energy Conversion, Shanghai Institute of Ceramics, Chinese Academy of Sciences, 1295 DingXi Road, Shanghai 200050, PR. China.

<sup>b</sup> University of Chinese Academy of Sciences, 19 A Yuquan Road, Beijing 100049, PR. China

\*Corresponding author

Shanghai Institute of Ceramics, Chinese Academy of Sciences, 1295 DingXi Road, Shanghai 200050, P. R. China

Tel: +86-21-52411704

Fax: +86-21-52413903

E-mail: [zywen@mail.sic.ac.cn](mailto:zywen@mail.sic.ac.cn)

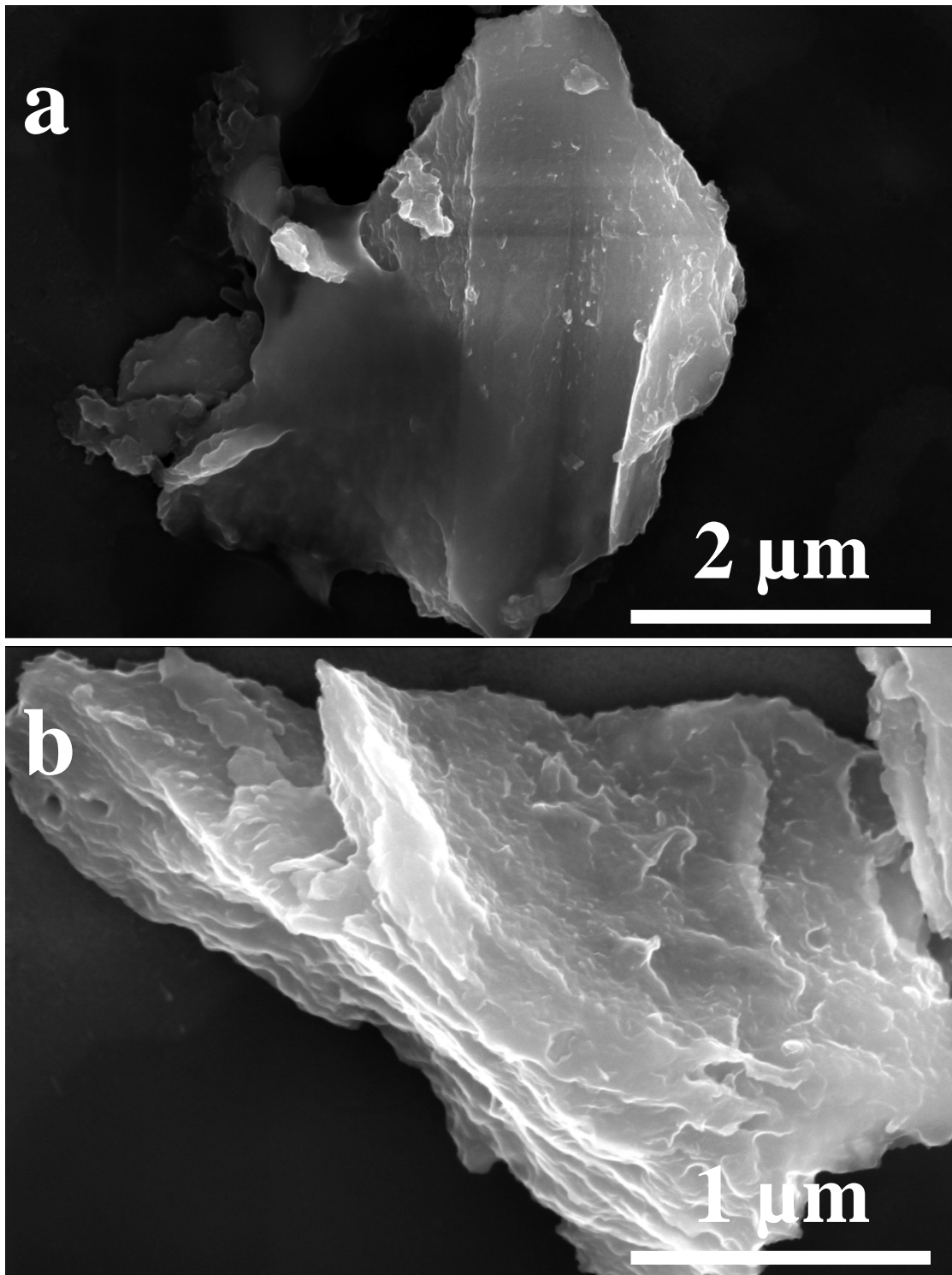


**Fig. S1** (a-b) SEM secondary electronic images of the FLD-MoS<sub>2</sub>/NC.

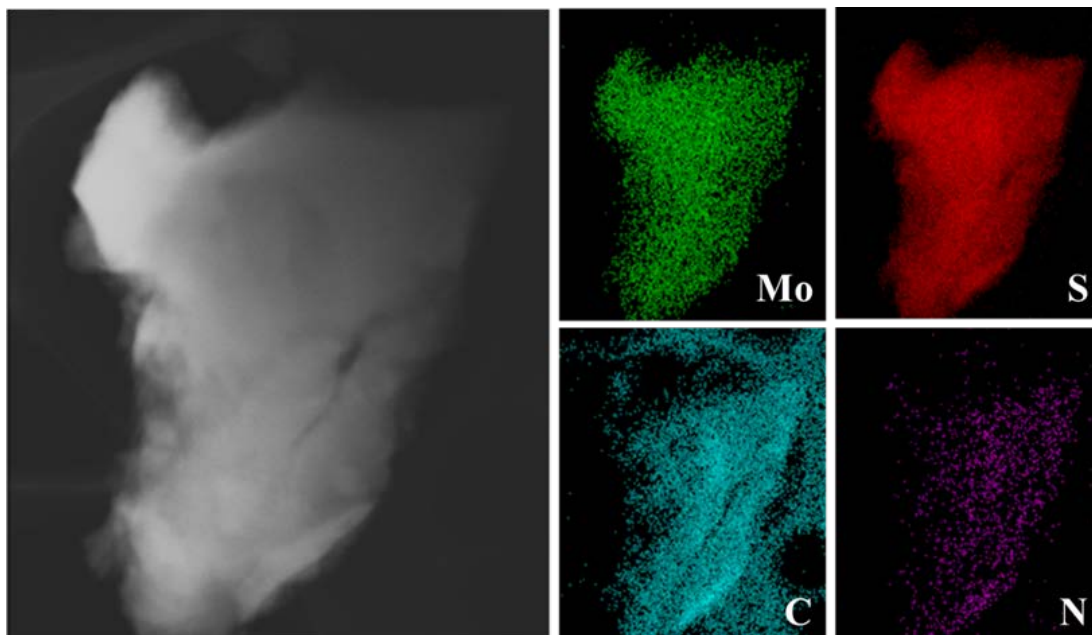


**Fig. S2** Electronic image and the corresponding elemental mapping analysis of the FLD-MoS<sub>2</sub>/NC.

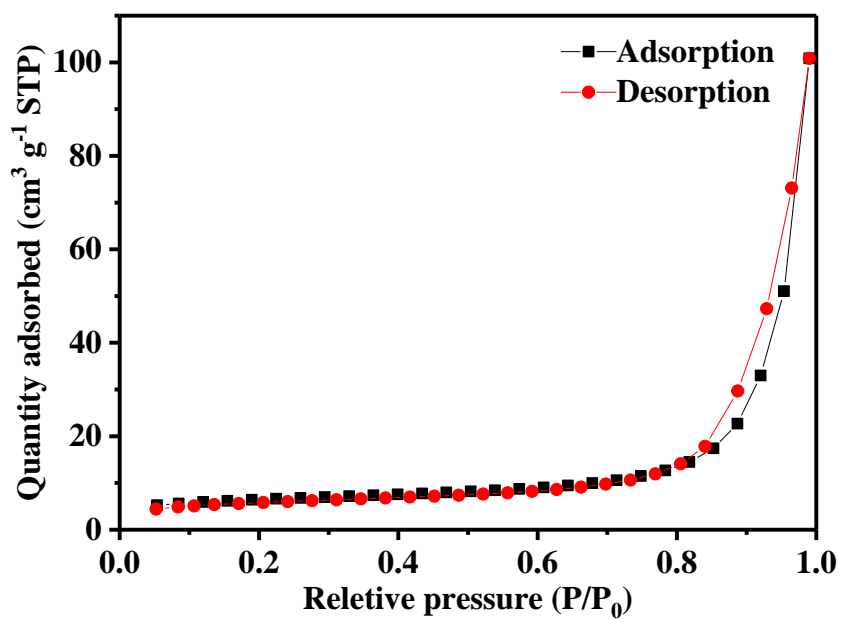


**Fig. S3** The N<sub>2</sub> adsorption-desorption isotherm of the FLD-MoS<sub>2</sub>/NC.

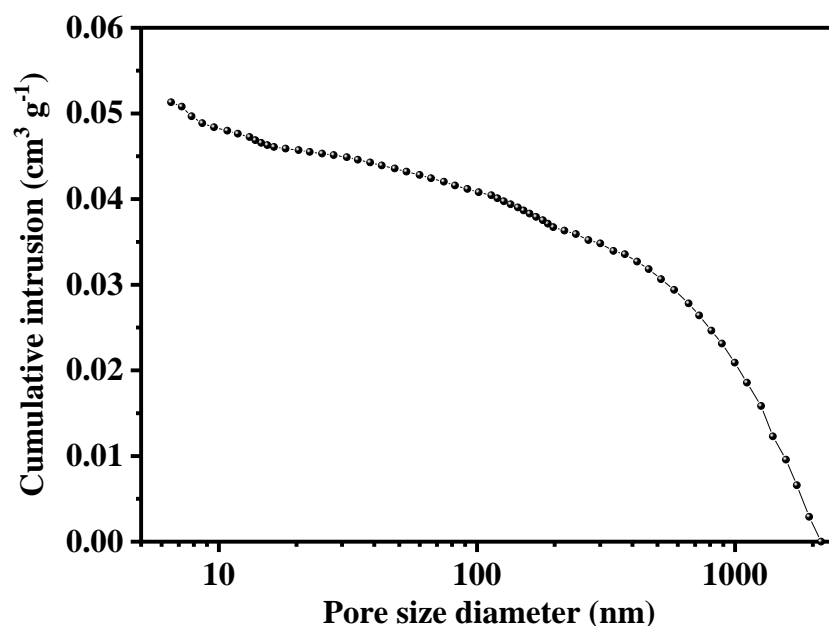


**Fig. S4** The curve of cumulative intrusion vs. pore size of the FLD-MoS<sub>2</sub>/NC.

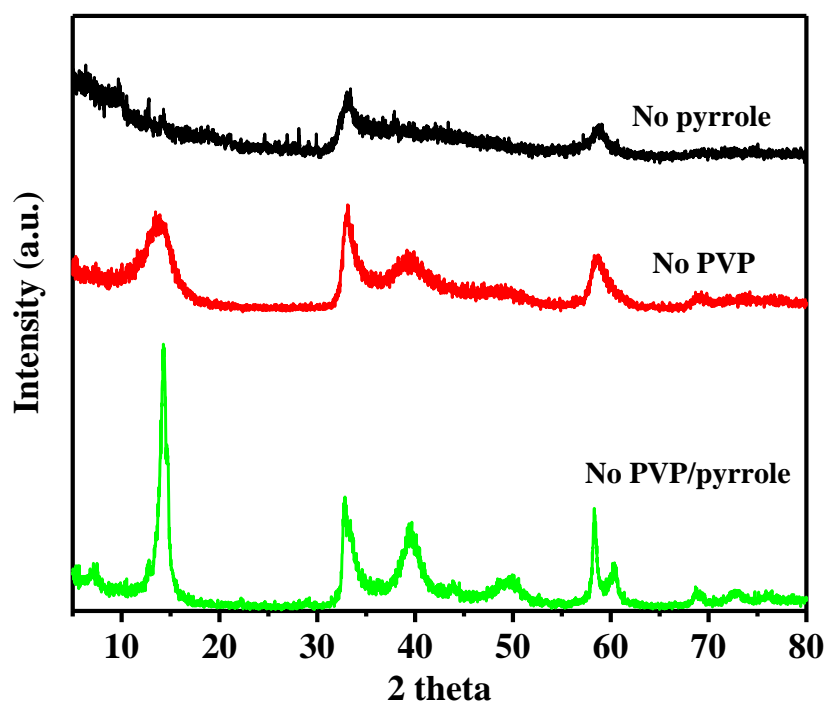


**Fig. S5** XRD patterns of the samples without adding pyrrole monomer or PVP or both.

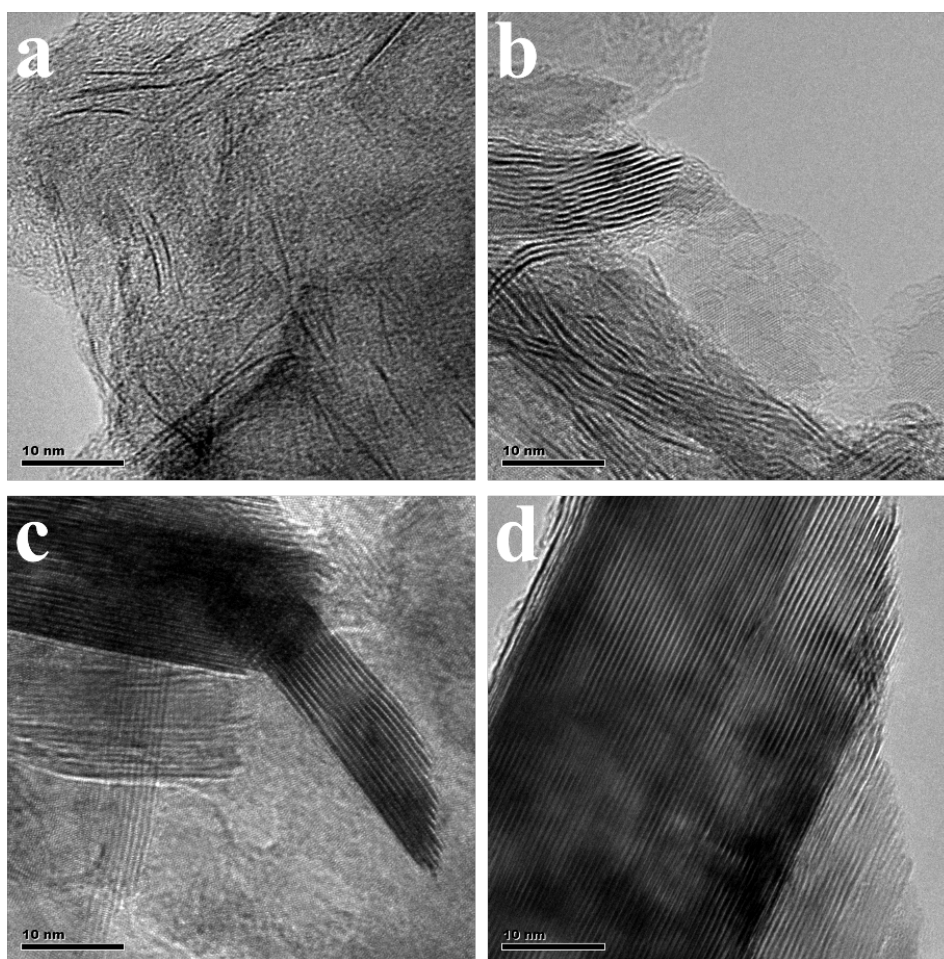


**Fig. S6** HR-TEM images of the comparison among (a) MoS<sub>2</sub>-no pyrrole, (b) MoS<sub>2</sub>-no PVP, (c) MoS<sub>2</sub>-no PVP/pyrrole and (d) commercial MoS<sub>2</sub>.

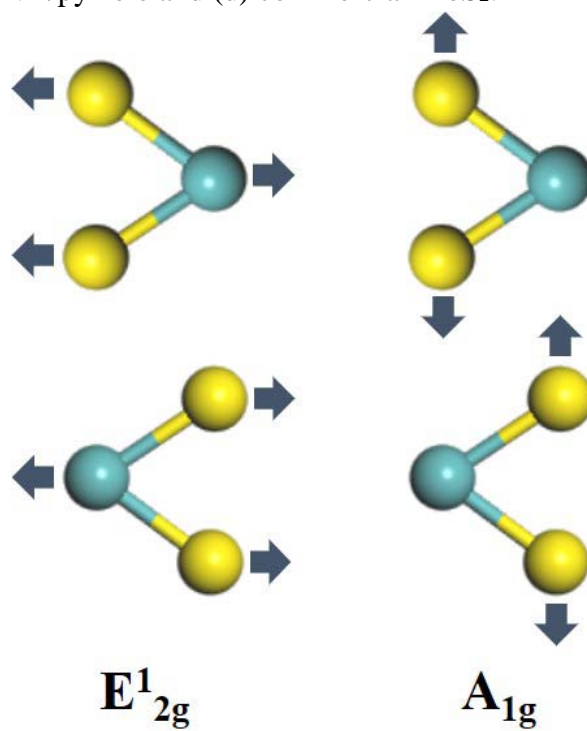


**Fig. S7** Illustration of  $E_{2g}^1$  and  $A_{1g}$  vibration modes of MoS<sub>2</sub>.

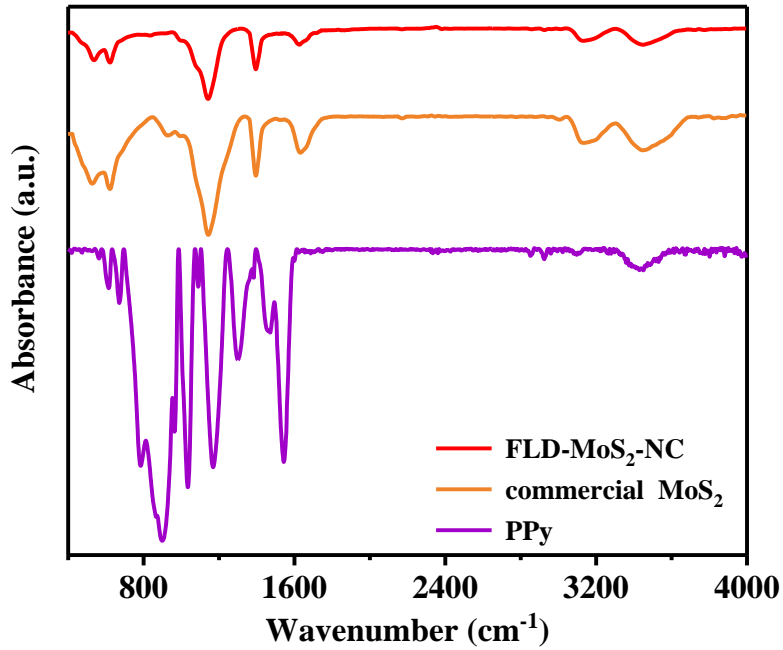


**Fig. S8** FTIR analysis of the FLD-MoS<sub>2</sub>/NC, commercial MoS<sub>2</sub> and PPy.

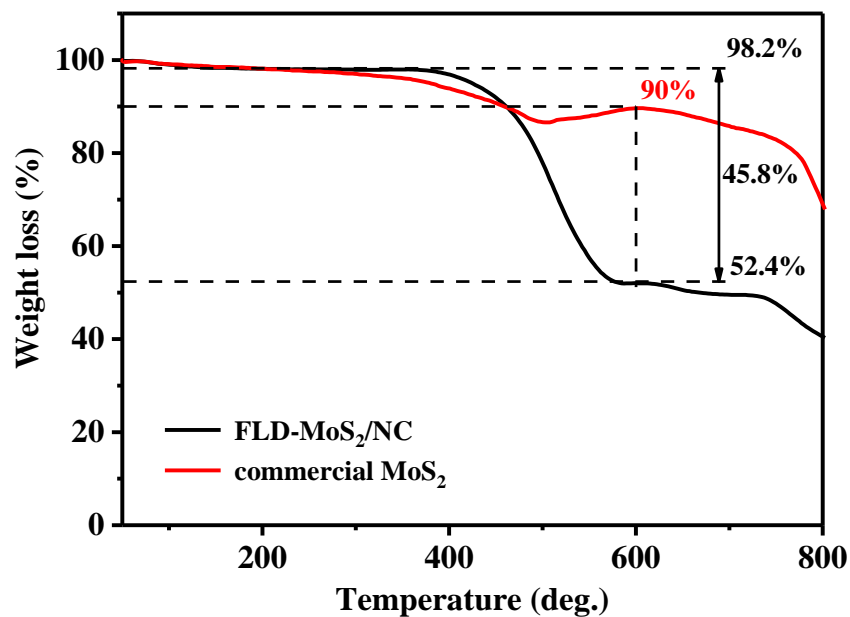


**Fig. S9** TG analysis of FLD-MoS<sub>2</sub>/NC and commercial MoS<sub>2</sub>.

From 300 °C to 600 °C, an obvious weight loss of 45.8% can be observed for the FLD-MoS<sub>2</sub>/NC. For commercial MoS<sub>2</sub> during the same temperature range, the weight loss is 8.2%. Then the weight ratio of the N-doped carbon in the FLD-MoS<sub>2</sub>/NC is calculated to be 40.96%. The calculation is presented as follows. Set the weight ratios of MoS<sub>2</sub> and N-doped carbon as  $\omega_1$  and  $\omega_2$ , respectively. Then we have the following equations.

$$\begin{aligned}\omega_1 + \omega_2 &= 100\% \\ \omega_1 \times 8.2\% + \omega_2 &= 45.8\%\end{aligned}$$

Finally, we can calculate that the weight ratio of N-doped carbon ( $\omega_2$ ) is 40.96%.

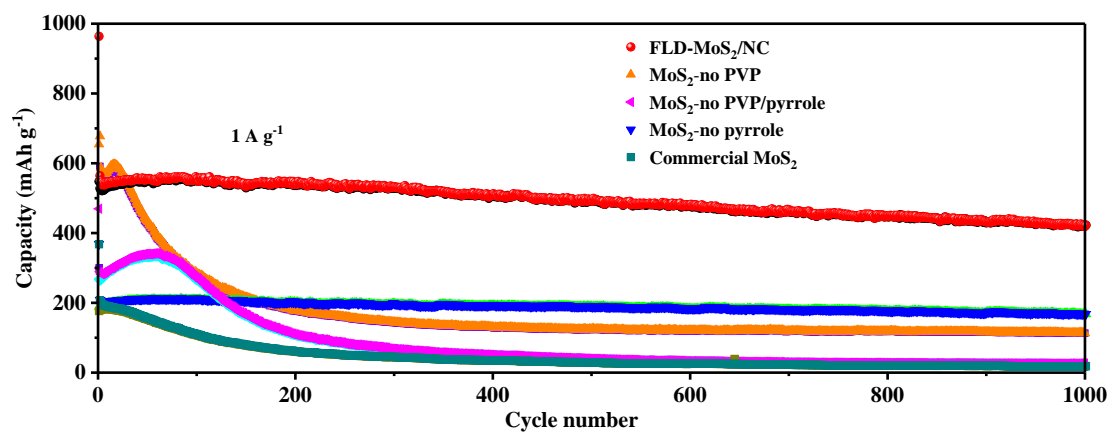


**Fig. S10** Cycle performance comparison among FLD-MoS<sub>2</sub>/NC, MoS<sub>2</sub>-no PVP, MoS<sub>2</sub>-no PVP/pyrrole, MoS<sub>2</sub>-no pyrrole and commercial MoS<sub>2</sub>. The current density is 1 A g<sup>-1</sup>.

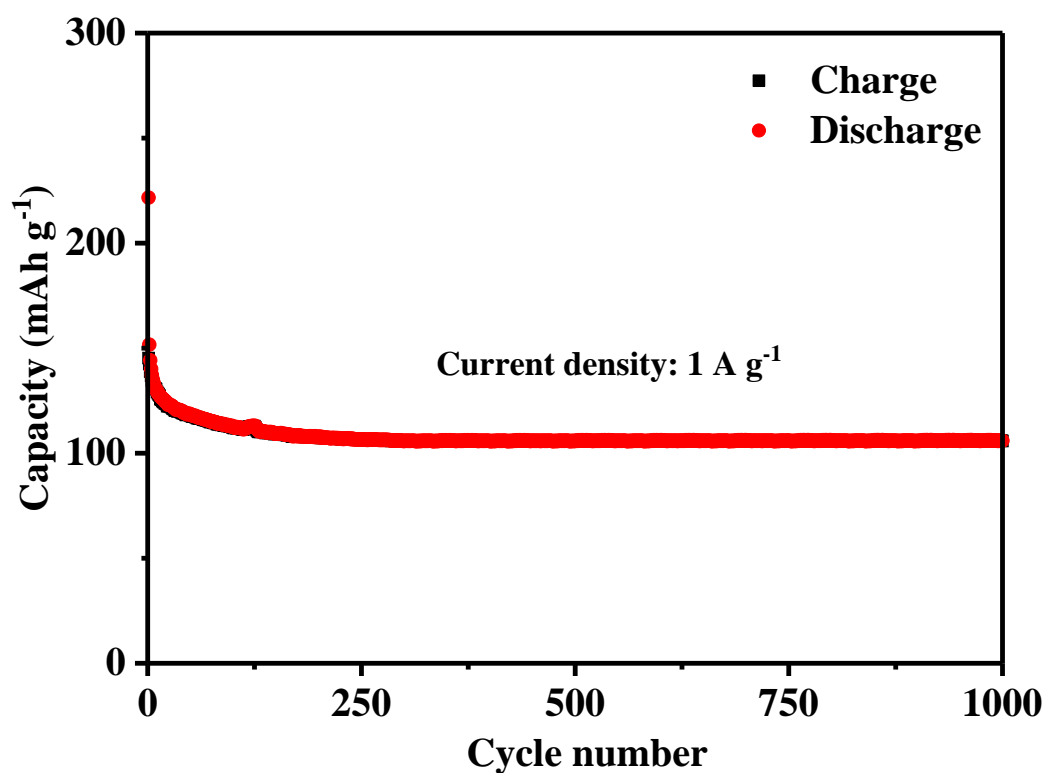


**Fig.S11** The sodium storage performance of the carbon matrix at the current density of 1 A g<sup>-1</sup>.

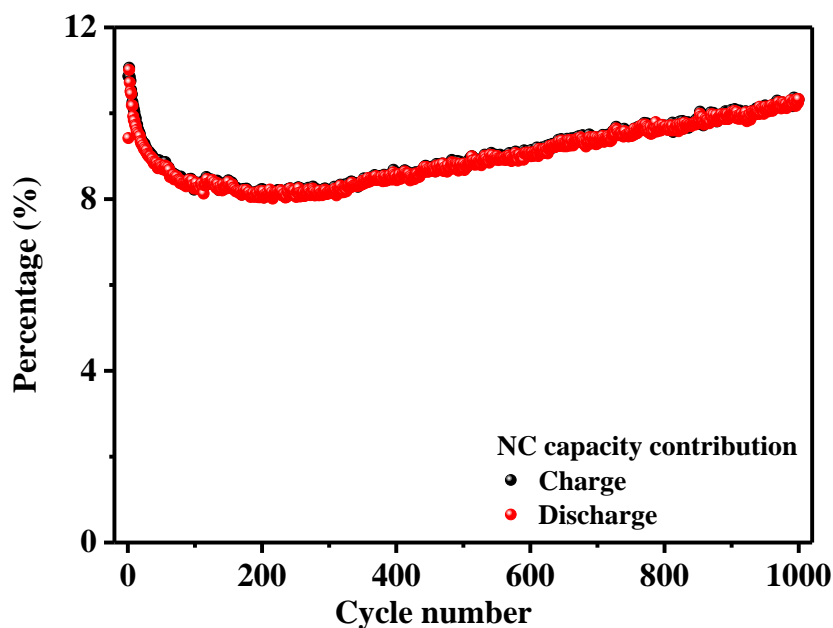


**Fig. S12** Percentage of NC contribution to the capacity of FLD-MoS<sub>2</sub>/NC at 1 A g<sup>-1</sup>. For the purpose of consistency, the electrode of N-doped carbon matrix was also prepared in the weight ratio of 70 wt.% active material, 20 wt.% Super-P conductive carbon black and 10 wt.% PVDF binder. The capacity was normalized to the weight of active material. The calculation of NC contribution is presented as follows. Set the experimental specific capacities of FLD-MoS<sub>2</sub>/NC and NC as C and C<sub>N</sub>, respectively. The masses of FLD-MoS<sub>2</sub>/NC and NC are set as m and m<sub>N</sub>, respectively. The weight ratio of NC is ω<sub>N</sub>. Then the NC contribution to the capacity (W) should be expressed as the equation below.

$$W = \frac{C_N m_N}{C m} = \frac{C_N}{C} \omega_N$$

The values of C, C<sub>N</sub> and ω<sub>N</sub> can be obtained from Fig. 4c, Fig. S11 and Fig. S9, respectively. Then the NC contribution to the capacity at 1 A g<sup>-1</sup> is presented below. It can be seen that during the 1000 cycles at 1 A g<sup>-1</sup>, the NC contribution to the whole capacity is in the range from 8% to 11%.

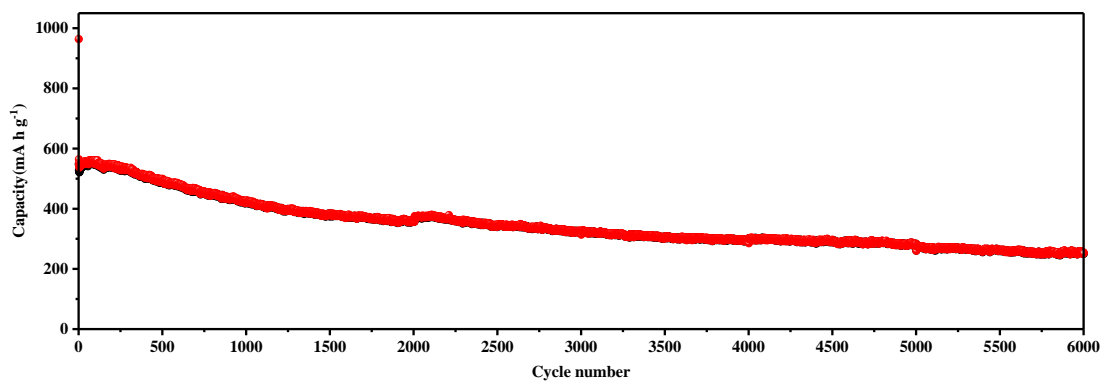


**Fig. S13** Prolonged cycle performance of FLD-MoS<sub>2</sub>/NC at 1A g<sup>-1</sup>.

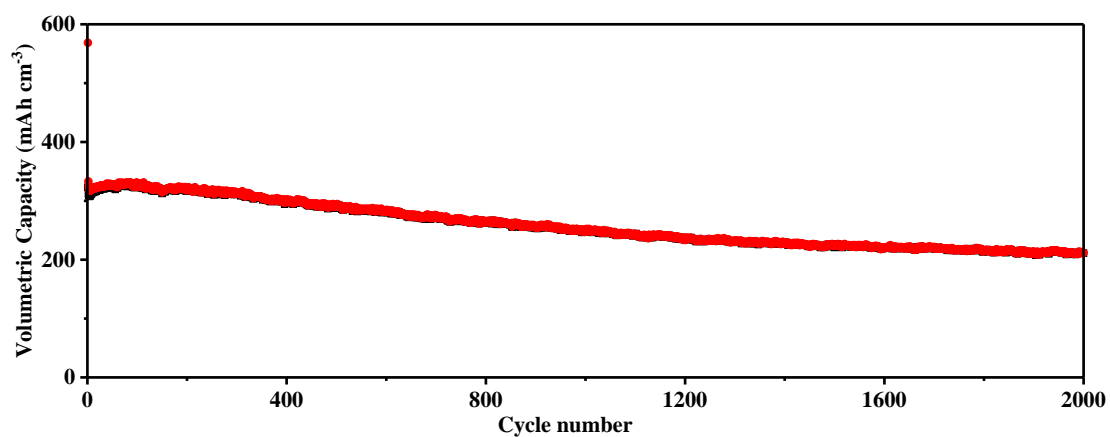


**Fig. S14** Cycle performance based on volumetric capacity of the FLD-MoS<sub>2</sub>/NC.

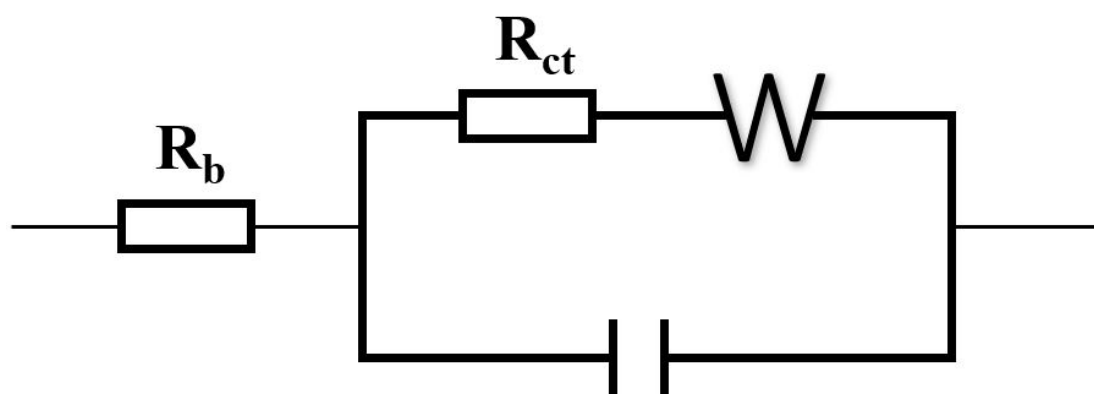


**Fig. S15** The equivalent circuit for EIS analysis.

	$R_b$	$R_{ct}$
FLD-MoS <sub>2</sub> /NC	9.89 $\Omega$	152 $\Omega$
MoS <sub>2</sub> without NC	12.3 $\Omega$	691 $\Omega$

**Table S1** EIS analysis of the FLD-MoS<sub>2</sub>/NC and MoS<sub>2</sub> without NC after cycling.

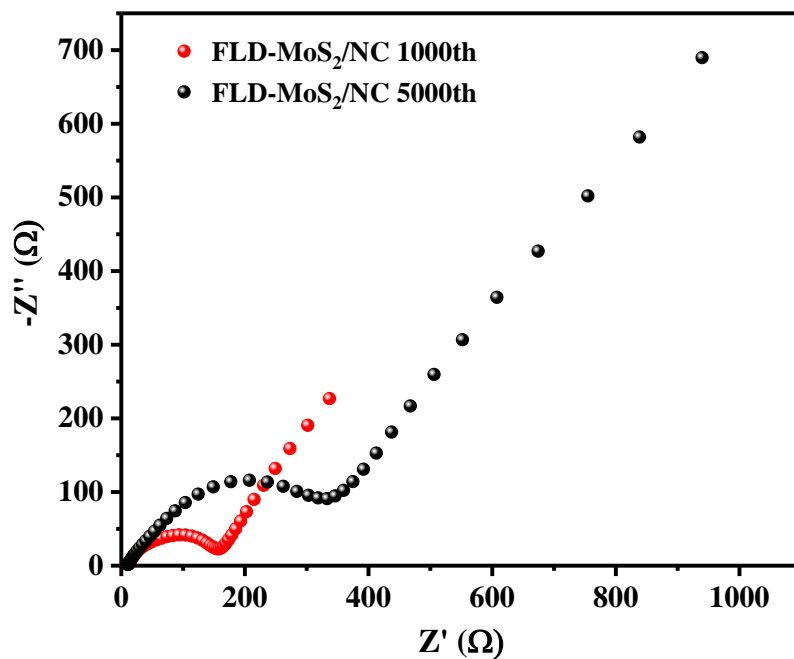


**Fig. S16** Nyquist plot of the FLD-MoS<sub>2</sub>/NC after 1000 and 5000 cycles at 1 A g<sup>-1</sup>.

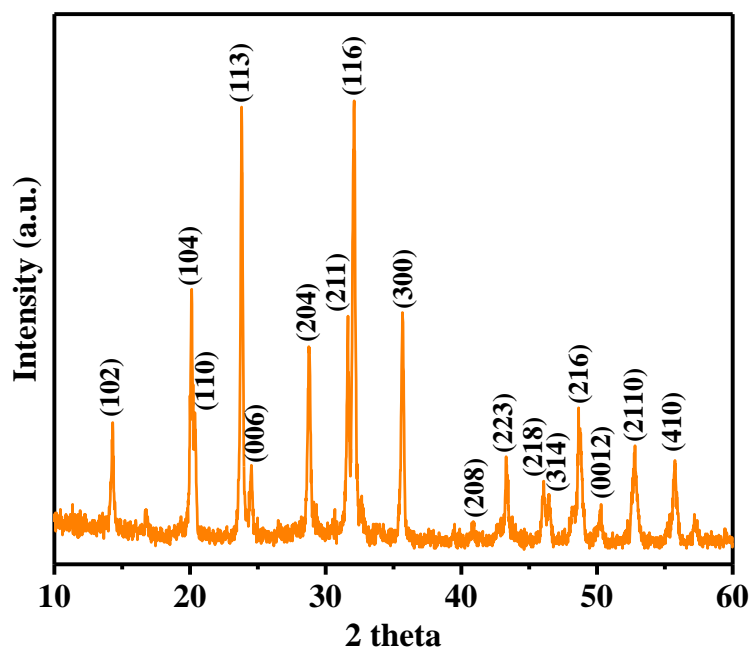


**Fig. S17** XRD pattern of the NVP/C.

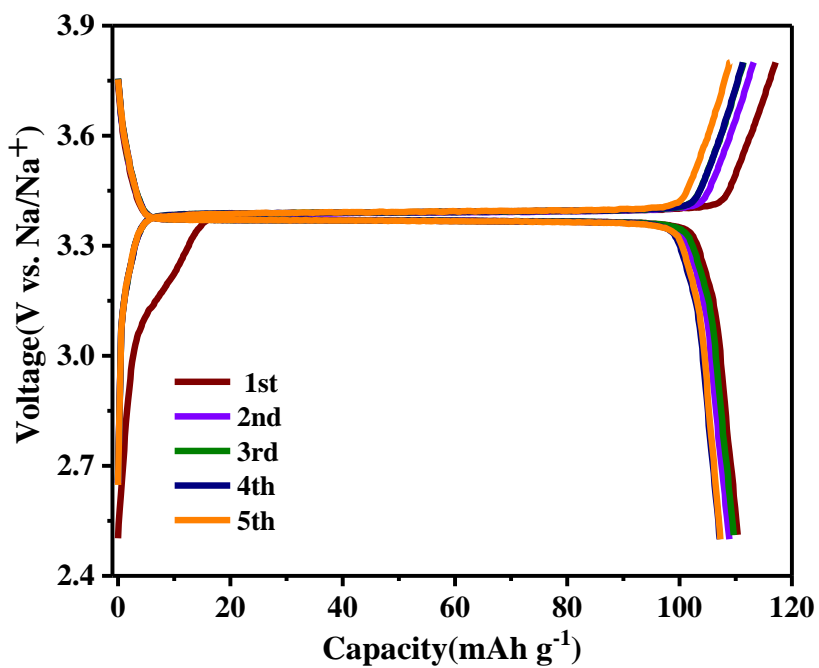


**Fig. S18** Charge-discharge curves of the NVP/C at 0.1 C for the initial 5 cycles in Na half-cell.

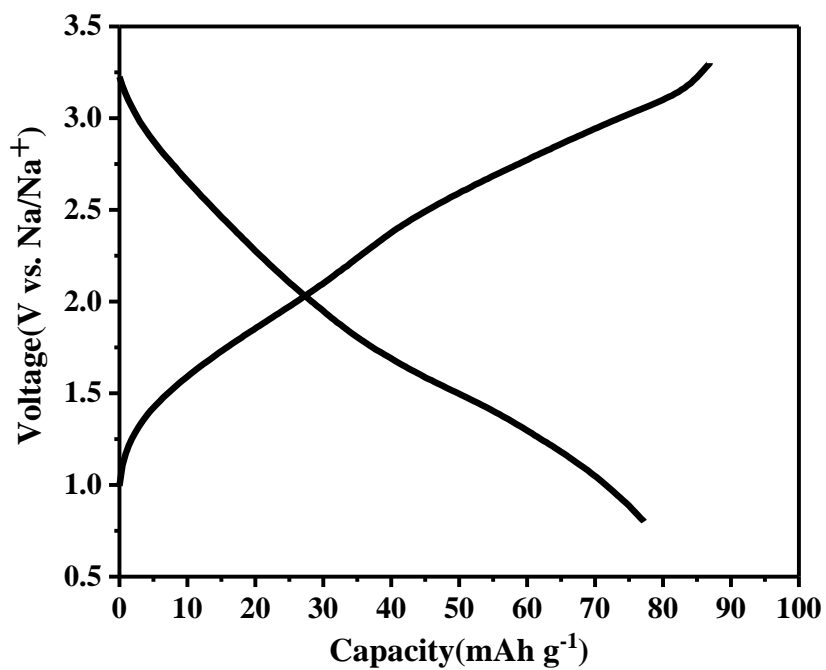


**Fig. S19** Initial charge-discharge curves of Na-ion full cell at 0.1 C.

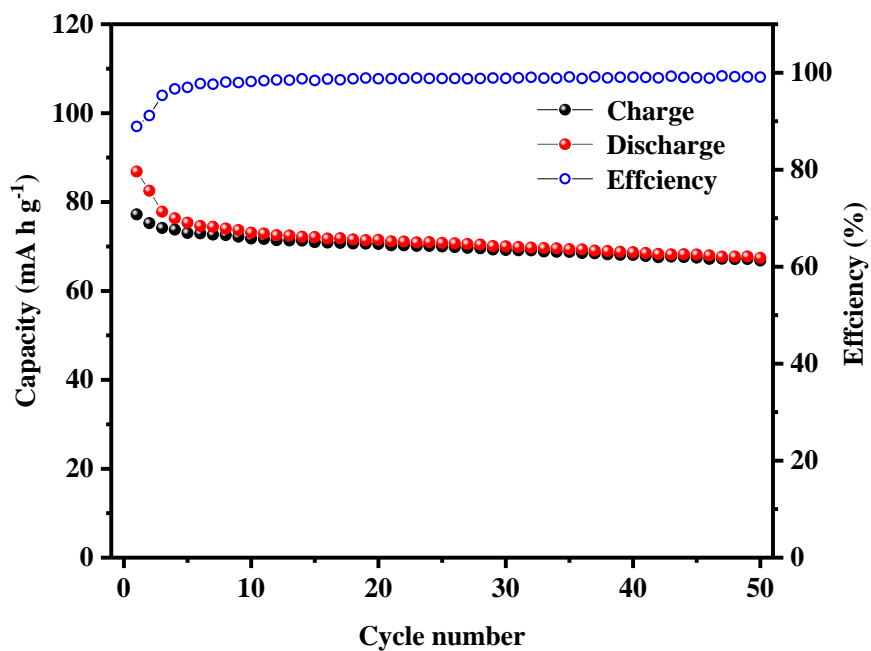


**Fig. S20** Cycle performance of Na-ion full cell at 0.1 C.

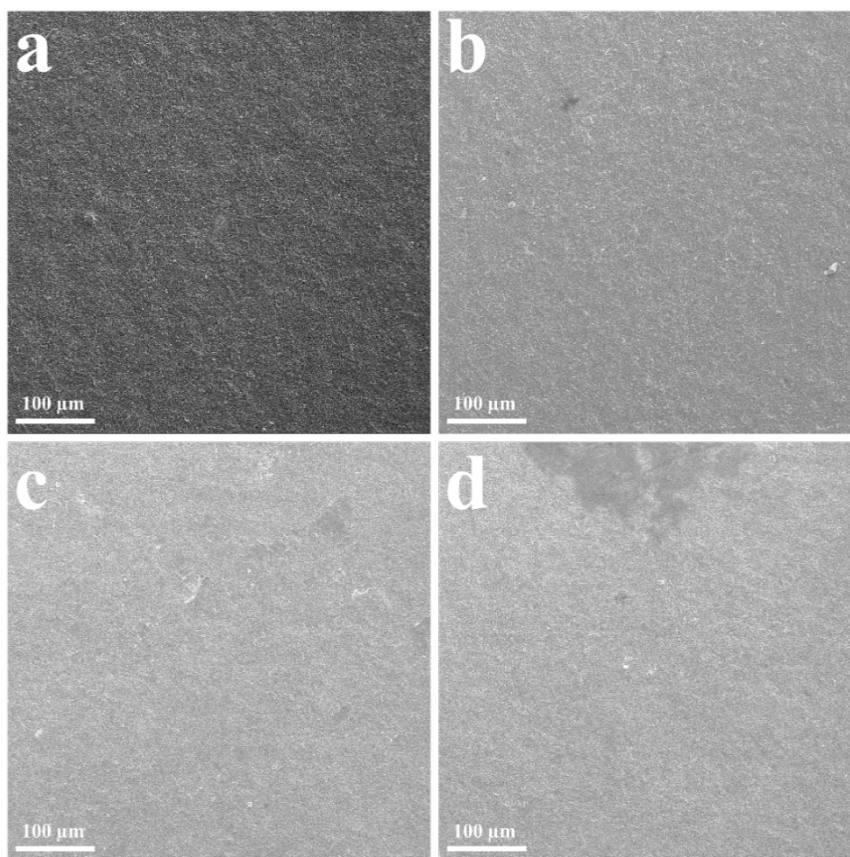


**Fig. S21** SEM images of electrodes before cycling: (a) FLD-MoS<sub>2</sub>/NC, (b) MoS<sub>2</sub>-no pyrrole (c) MoS<sub>2</sub>-no PVP and (d) MoS<sub>2</sub>-no PVP/pyrrole.